Available online at www.sciencedirect.com
SCIENCE DIRECT®
Journal of the European Ceramic Society 25 (2005) 1771–1780
www.elsevier.com/locate/jeurceramsoc

Short-term oxidation of a ternary composite in the system AlN–SiC–ZrB_2

Mylène Brach, Diletta Sciti*, Andrea Balbo, Alida Bellosi

CNR-ISTEC, Institute of Science and Technology for Ceramics, Via Granarolo 64, I-48018 Faenza, Italy

Available online 23 January 2005

Abstract

The present study investigates the oxidation behaviour in air of a structural ceramic composite with the following volumetric composition: 55% AlN–15% SiC–30% ZrB_2. This kind of ternary composite is electroconductive (3×10^{-4} Ω cm) and has significant strength (~700 MPa) and toughness (4 MPa $m^{1/2}$) up to 1000 °C. Oxidation tests were carried out in a TG equipment from 700 to 1300 °C with exposition time of 30 h. Significant weight gain is observed at $T > 1000$ °C. In the range 700–900 °C, the process is dominated by the oxidation of ZrB_2 into zirconia and boria and the kinetic is nearly parabolic. At temperatures in the range 1000–1100 °C, boria reacts with alumina forming aluminium borate and borosilicate glass and the kinetic largely deviates from parabolic behaviour. In the samples oxidized at temperatures in the range 1200–1300 °C, aluminium borate and mullite crystallize on the surface. The kinetics is para-linear in this temperature range but at 1300 °C, the rupture of the outer layer, results in accelerated damage of the sample. The composite is recommended for applications up to 1100 °C.

Keywords: Composites; Corrosion; ZrO_2; Microstructure; AlN–SiC–ZrB_2

1. Introduction

Ternary ceramic composites constituted by a matrix of AlN + SiC and containing an amount of ZrB_2 phase have shown to possess good mechanical properties up to 1300–1400 °C and electro-conductivity.[1] Therefore, possible applications for these materials are heaters and igniters, provided they have an adequate oxidation resistance. However, strength tests conducted at 1300 °C revealed a marked surface degradation due to oxidation effects. The composites are constituted by three oxidizable phases, namely AlN, which is the main constituent (55 vol.%), SiC (10 vol.%) and ZrB_2 (30 vol.%).

At temperatures above 600 °C, monolithic AlN reacts with oxygen forming alumina which can be amorphous at $T < 1000$ °C and becomes crystalline corundum at $T > 1000$ °C. Different kinetic models have been proposed in literature for the oxidation of AlN depending on time, temperature, oxidizing atmosphere and characteristics of the samples. A parabolic behaviour is reported by Lavrenko and Alexeev[2] and oxygen diffusion is indicated as the rate controlling mechanism. In contrast, in the work of Bellosi et al.,[3] the alumina scale was found to be non-protective, due to porosity, and consequently the kinetics is linear. Kim and Moorhead[4] found parabolic weight gains for temperature $T = 1200$ °C linear weight gains at higher temperatures.

SiC is a very stable phase due to the development of a SiO_2 protective layer. It was found by several studies that at the beginning of oxidation and at low temperatures the oxidation product is amorphous, while after long exposures or higher temperatures, it tends to crystallise.[5,6] It is generally recognized that the oxidation rate decreases with time following a parabolic or nearly parabolic behaviour. However, the rate of oxidation is not exclusively controlled by diffusion of oxygen but can be affected by CO diffusion or interface reaction.[7]

A parabolic behaviour was reported for the oxidation of ZrB_2 up to 1100 °C,[4–8] due to formation of ZrO_2 and liquid boria, B_2O_3, which acts as an effective barrier against oxygen

* Corresponding author. Tel.: +39 0546699748; fax: +39-054646381.
E-mail address: dile@istec.cnr.it (D. Sciti).

0955-2219/$ – see front matter © 2004 Elsevier Ltd. All rights reserved.
doi:10.1016/j.jeurceramsoc.2004.12.007

diffusion. At higher temperature, B_2O_3 starts to vaporize notably, and the ZrO_2 porous layer is no longer protective. In order to overcome this problem, it was shown that the addition of SiC is highly beneficial for improving ZrB_2 oxidation resistance at temperature >1200 °C, thanks to the formation of a protective borosilicate glass.[9–11] In the present work, the oxidation behaviour of the ternary AlN–SiC–ZrB_2 composite is expected to be affected by competitive mechanisms such as the accelerated oxidation of ZrB_2 into ZrO_2 (non-protective) and the formation of protective oxides, e.g. mullite, resulting from oxidation of the AlN/SiC matrix.

2. Experimental procedure

2.1. Material

The dense ceramic composite was produced from the following commercial powders: AlN Grade C powder (H.C. Starck, Berlin, Germany) with d_{50} = 2.29 μm, oxygen content of 1.8 wt.% and specific surface area of 4.3 m^2/g; SiC BF-12 (H.C. Starck, Berlin, Germany) with 97 wt.% of β-SiC, mean particle size 0.23 μm, oxygen content of 0.88% and specific surface area of 12 m^2/g; ZrB_2 Grade B (H.C. Starck), grain size range 0.1–8 μm, oxygen content 1 wt.%. The composition 55 vol.% AlN + 15 vol.% SiC + 30 vol.% ZrB_2 was selected on the basis of preliminary experiments. The powder mixture was prepared by ball milling for 24 h in absolute ethanol using silicon nitride balls. The slurry was dried in a rotary evaporator and sieved. Sintering was performed through hot pressing at 1870 °C, with an applied pressure of 30 MPa and 10 min holding time, in vacuum. The final density was determined with the Archimede's method. Microstructural features and mechanical properties are described below.

2.2. Oxidation tests

Rectangular plates 9.0 mm × 8.0 mm × 1.0 mm were used for oxidation tests. The surface was mechanically ground and the measured surface roughness is about 1.02 μm. The specimens were cleaned in ultrasonicated acetone bath, dried and weighed (accuracy 0.01 mg). The oxidation tests were carried out in a Thermogravimeter analyser (model STA449, NETSCH, Geraetebau GmbH, Germany), in synthetic air (composition: 80 vol.% N_2 + 20 vol.% O_2, with 30 ml/min gas flow) between 700 and 1300 °C with isothermal exposition time of 30 h for each experiment, heating rate 30 °C/min and free cooling. The fast heating up stage prior to the isothermal period was applied to minimize oxidation effects before reaching the target temperatures. The specimens were placed inside an Al_2O_3 vertical heated chamber on an Al_2O_3 TG-plate. The mass variation was recorded continuously with 10^{-3} mg of accuracy. The TG measurements evaluation is performed with subtraction of the Buoyancy effect corrections.

Oxidised and as-sintered sample surfaces were analysed by X-ray diffraction (Cu Kα radiation, Miniflex Rigaku, Tokyo, Japan). Sample surfaces and polished cross-sections were analyzed by scanning electron microscope (SEM, Model Cambridge S360) and energy dispersive microanalysis (EDX, Model INCA energy 300; Oxford Instruments, UK).

3. Results

3.1. Microstructure and mechanical properties of the as-sintered material

The hot pressed composite approached the theoretical density (relative density >99%). An example of the sample surface is shown in Fig. 1. Crystalline phases determined with X-ray diffraction are AlN, SiC and ZrB_2. The microstructure presented in Fig. 1 reveals bright particles that correspond to zirconium diboride, whereas the dark phase is composed of AlN and SiC, which are not distinguishable neither in secondary electron images nor in backscattered electron images (due to the very close atomic number). Mechanical properties of the hot pressed composite are given in Table 1.

3.2. Oxidation kinetics

The total weight gain measured on the oxidized samples and the thickness of the oxidised layer (measured on the SEM micrographs of the polished cross-sections) are shown in Fig. 2a and b. The oxidized samples do gain very little weight from 600 °C up to 1100 °C, whereas at oxidation temperatures above 1200 °C the weight gain and the oxide scale thickness increase rapidly. An anomalous behaviour was observed for the oxidation at 1000 °C, where the weight gain is slightly lower compared to treatment at 900 °C.

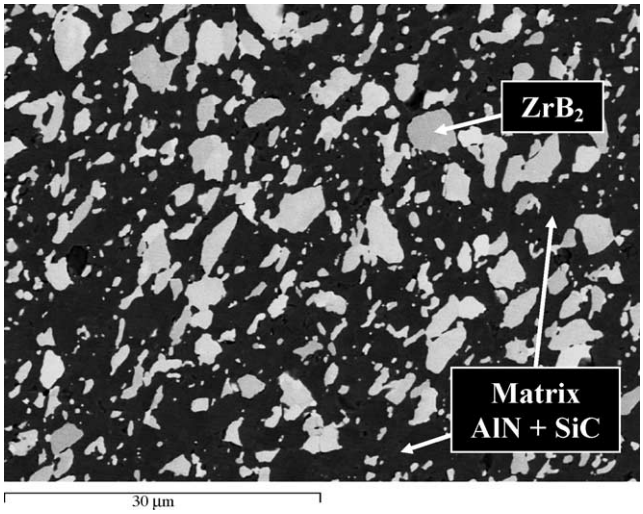

Fig. 1. Microstructure of the as-sintered sample.

Table 1
Characteristics of the starting material

Sintering cycle (°C/min)	1870/10
Relative density (%)	99.5
E (GPa)	366
HV (GPa)	15.6 ± 0.4
K_{Ic} (MPa m$^{1/2}$)	4.0 ± 0.1
σ (RT) (MPa)	671 ± 166
σ (1000 °C) (MPa)	615 ± 121
σ (1300 °C) (MPa)	525 ± 29
σ (1400 °C) (MPa)	508 ± 33

E: Young's modulus (resonance frequency method); HV: Vickers hardness (9.81 N load); K_{Ic}: fracture toughness (Chevron-notched beam in flexure); σ: 4-point flexual strength (25 mm × 2 mm × 2.5 mm test bars, lower span 20 mm, upper span 10 cm).

Given the complexity of the system, including three oxidizable phases, a simple parabolic law is unable to describe the kinetic behaviour, as many different processes affecting the kinetics are expected to occur. Therefore, in order to give a complete analytical description, the curves were fitted according to a multiple-law model[12] including a linear, parabolic and logarithmic term. The mass change per unit area w is expressed as a function of time, according to the following equation:

$$w = K_{\text{lin}} \cdot t + K_{\text{par}} \cdot \sqrt{t} + K_{\log} \cdot \log(t) \quad (1)$$

TG curves are presented in Fig. 3a–h, (relative to the isothermal run), and each graph shows the experimental data and the solution. The K parameters and R^2 values corresponding to each fitting curve are reported in Table 2.

In the range 700–900 °C, the best fitting solution is a mixed parabolic–linear law, where the dominating term is the parabolic one and the linear term is negative, accounting for mass loss due to vaporization of volatile species (Fig. 3a–c). The decelerated kinetic obtained at 1000 °C is not well fitted by Eq. (1). The most reasonable solution contains a logarithmic term, which is the dominating one, and a negative linear term, which can be related to release of volatile species, as explained below. The agreement between the fitting equation and the experimental data is good for $t > 4$ h during the isothermal run (Fig. 3d). The most realistic solutions for the kinetic curve relative to treatment at 1100 °C, is a multiple law containing all the terms of Eq. (1). In this case,

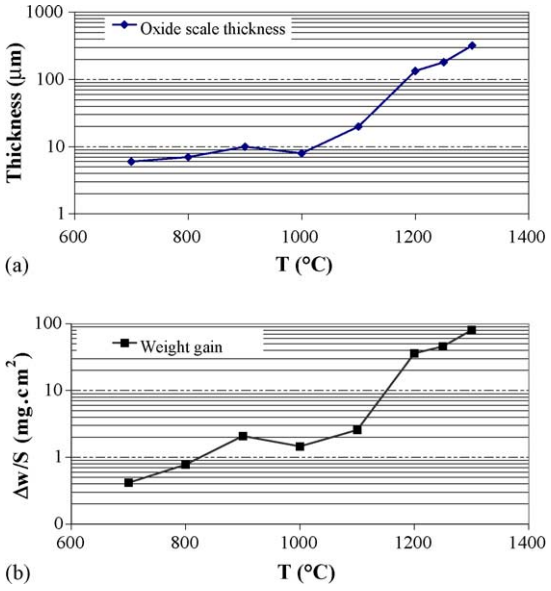

Fig. 2. (a) Oxide scale thickness and (b) weight gain of the samples, with respect to the oxidation temperature, measured after each oxidation test.

Table 2
Kinetic parameters of the oxidation fitting curve, relatively to parabolic (par), linear (lin) and logaritmic (log) contributions, and R^2 (fit goodness) values

Oxidation temperature (°C)	K_{par} (mg cm^{-2} min$^{-1/2}$)	K_{lin} (mg cm^{-2} min^{-1})	$K_{\log}$ (mg cm^{-2})	R^2
700	0.008	-3.9×10^{-5}	–	0.9986
800	0.02	-1.6×10^{-4}	–	0.9998
900	0.06	-5.8×10^{-4}	–	0.9993
1000	–	-9.2×10^{-5}	0.15	0.9992
1100	0.050	8.0×10^{-5}	0.195	0.9977
1200	0.27	7.9×10^{-3}	–	0.9999
1250	0.58	5.1×10^{-3}	–	0.9998
1300	0.76	1.3×10^{-2}	–	0.9997

Table 3
Crystalline phases detected by XRD on the as-sintered material and on the oxidized surfaces after the treatment for 30 h in the temperature range 700–1300 °C

	As-sintered	700 °C	800 °C	900 °C	1000 °C	1100 °C	1200 °C	1250 °C	1300 °C
ZrB_2	vs	s	w						
AlN	w	w	w	w	vw				
SiC	w	w	w	w	vw				
m-ZrO_2		w	s	vs	vs	vs	s	s	s
$2Al_2O_3 \cdot B_2O_3$				vw	w	s	vs	w	vw
$Al_{18}B_4O_{33}$								s	vs
Mullite							s	s	vs

vs, very strong; s, strong; w, weak; and vw, very weak.

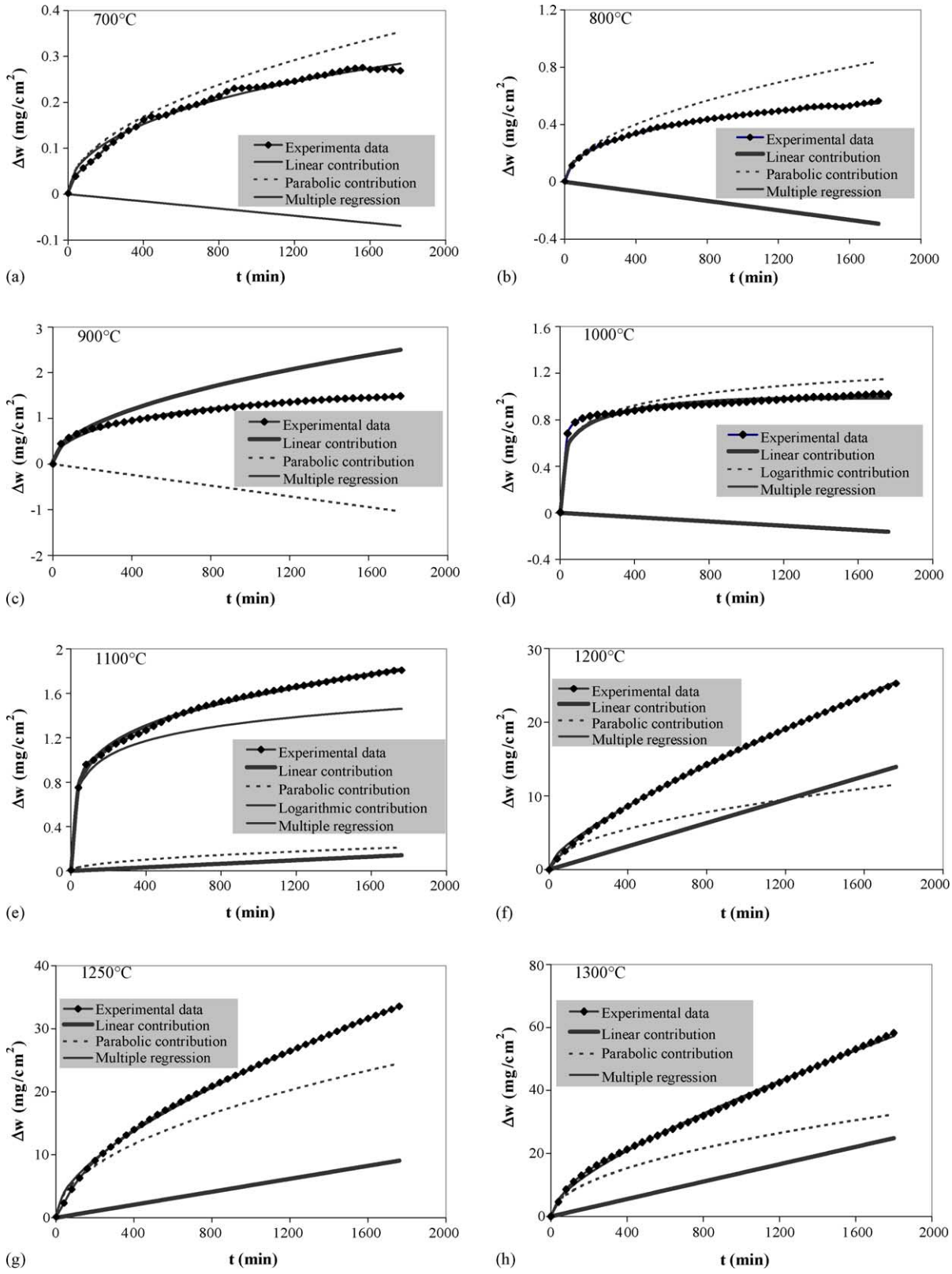

Fig. 3. Thermogravimetric curves (point graph) of the samples at various oxidation temperatures: (a) 700 °C; (b) 800 °C; (c) 900 °C; (d) 1000 °C; (e) 1100 °C; (f) 1200 °C; (g) 1250 °C and (h) 1300 °C. The line graphs represent the mixed law model (Eq. (1)) and its single contributions.

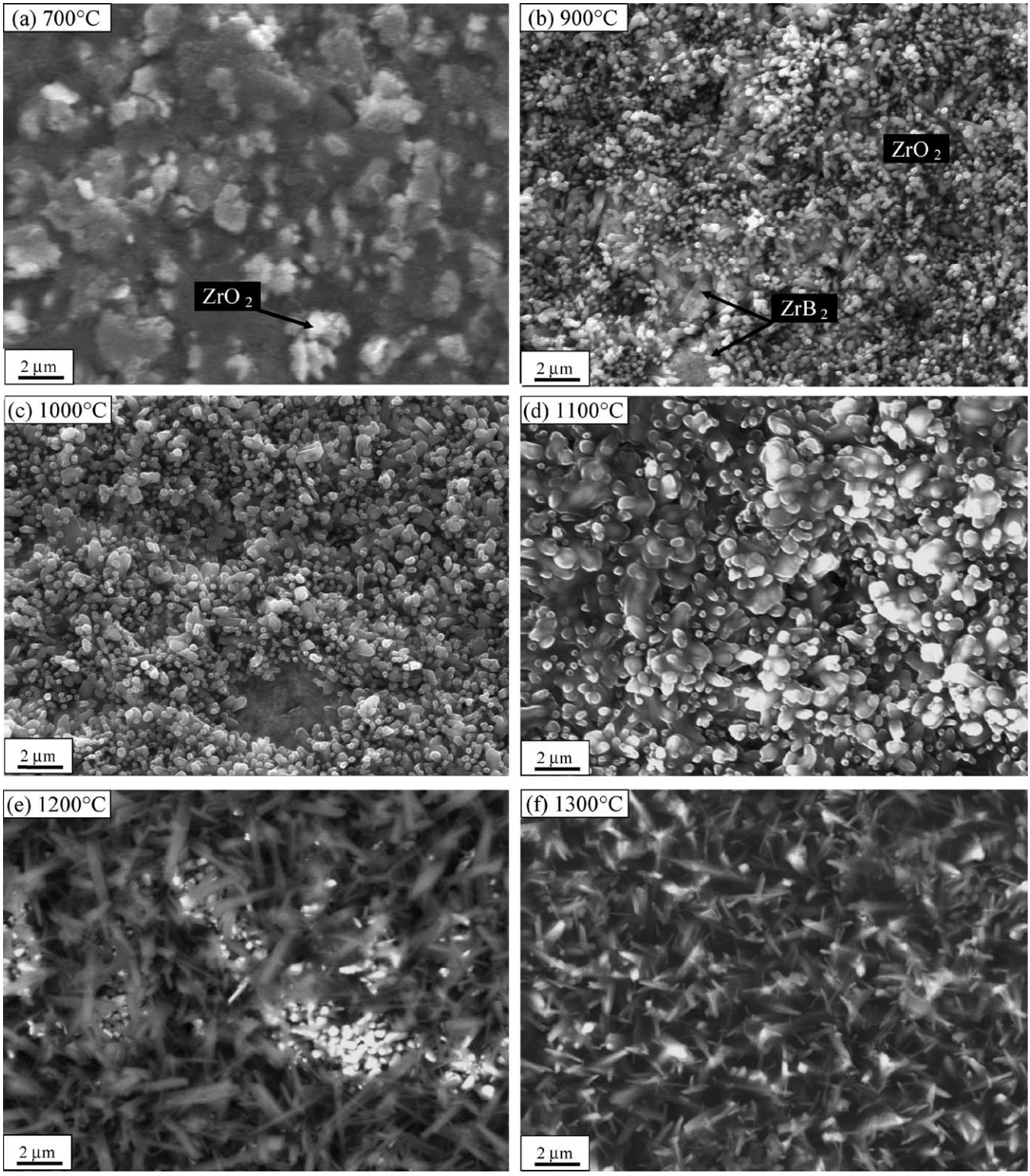

Fig. 4. SEM Micrographs of the sample surfaces after oxidation for 30 h at: (a) 700 °C; (b) 900 °C; (c) 1000 °C; (d) 1100 °C; (e) 1200 °C and (f) 1300 °C.

the dominating term is the logarithmic one (Fig. 3e). In the range 1200–1300 °C, the kinetic curves are best fitted with a parabolic plus linear law where the dominating terms are the parabolic ones (Fig. 3f–h).

3.3. Microstructure evolution due to oxidation

Crystalline phases detected by XRD on the as-sintered material on the oxidized surfaces are shown in Table 3. SEM micrographs in Figs. 4 and 5 show surfaces and cross-sections of the oxidized samples for selected temperatures.

The extent of oxidation in the temperature range 700–800 °C (Figs. 4a and 5a) is rather limited and only concerns the reaction of ZrB_2 into ZrO_2. The formation of zirconia involves volume expansion, which results in the fracture of ZrB_2 particles, with consequent formation of cracks that are visible only on the sample surface. X-ray diffraction patterns show that the amount of monoclinic ZrO_2 increases with increasing the oxidation temperature and that ZrO_2 crystals are oriented preferentially along the $(-1\,1\,1)$ plane.

In the samples oxidized at 900–1100 °C (Fig. 4b–d), the surface is covered by small crystals, located mainly in contact

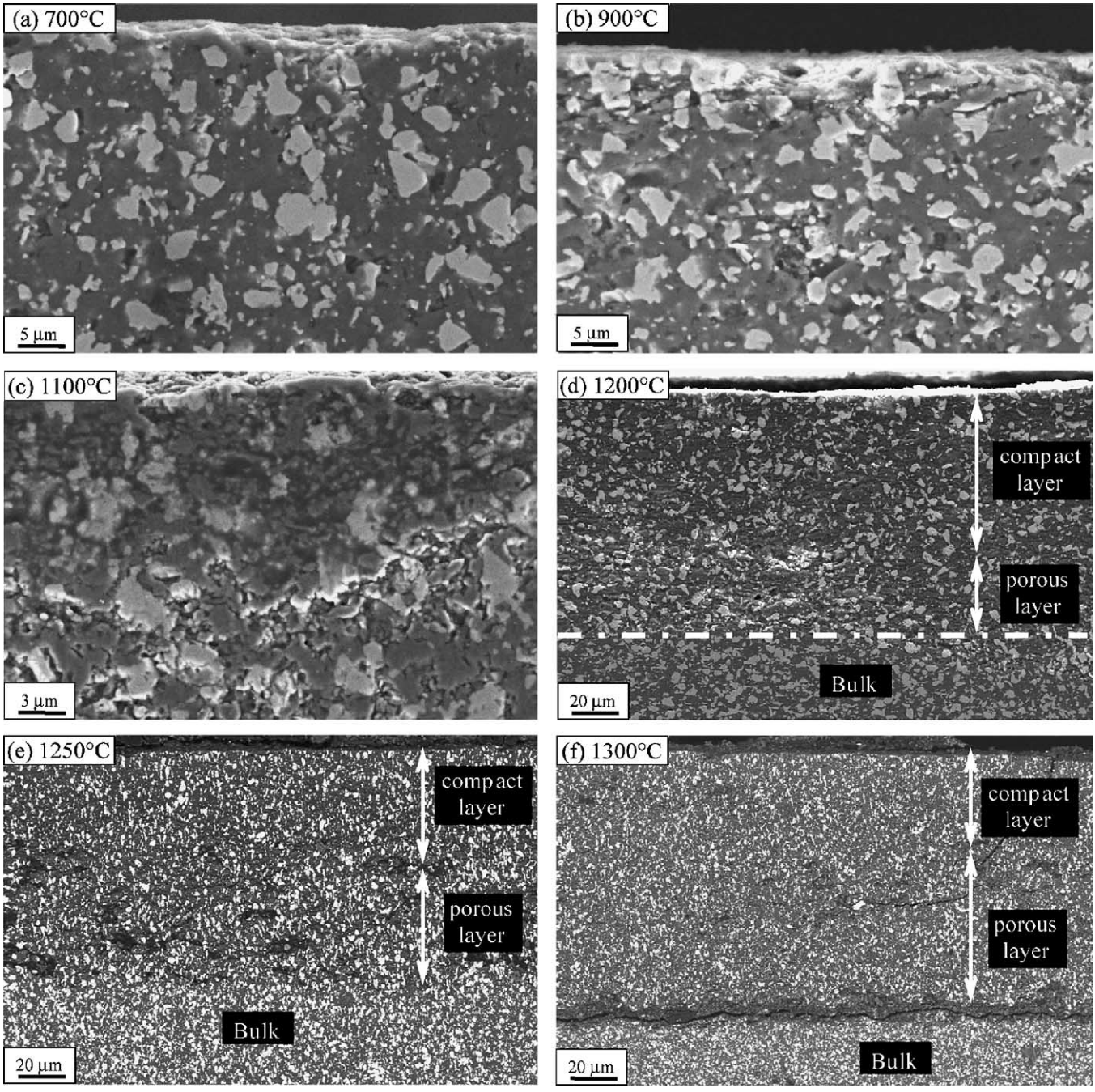

Fig. 5. SEM Micrographs of the cross-sections of the sample oxidised at: (a) 700 °C; (b) 900 °C; (c) 1100 °C; (d) 1200 °C; (e) 1250 °C and (f) 1300 °C.

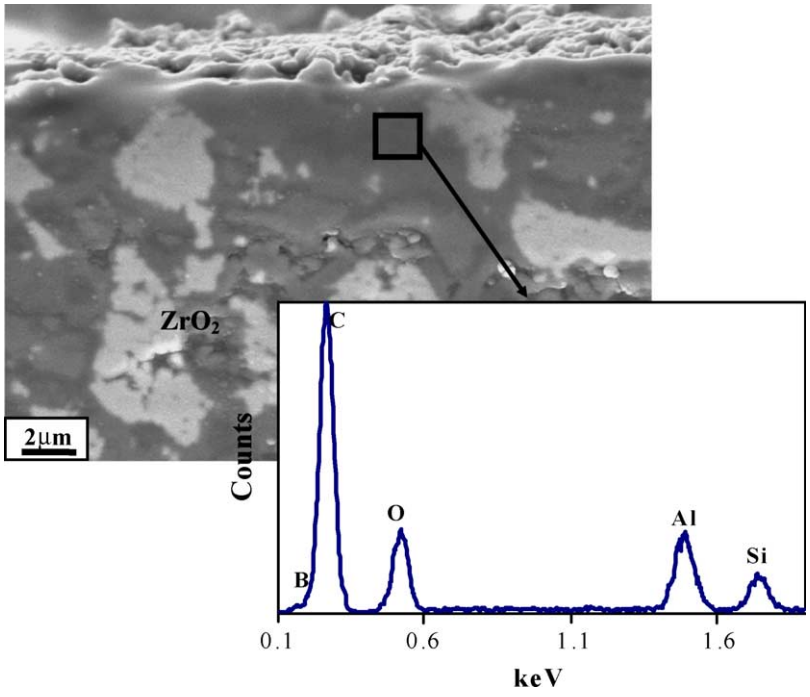

Fig. 6. SEM Micrograph of the cross-section and EDS Spectrum: glassy layer after oxidation at 1200 °C.

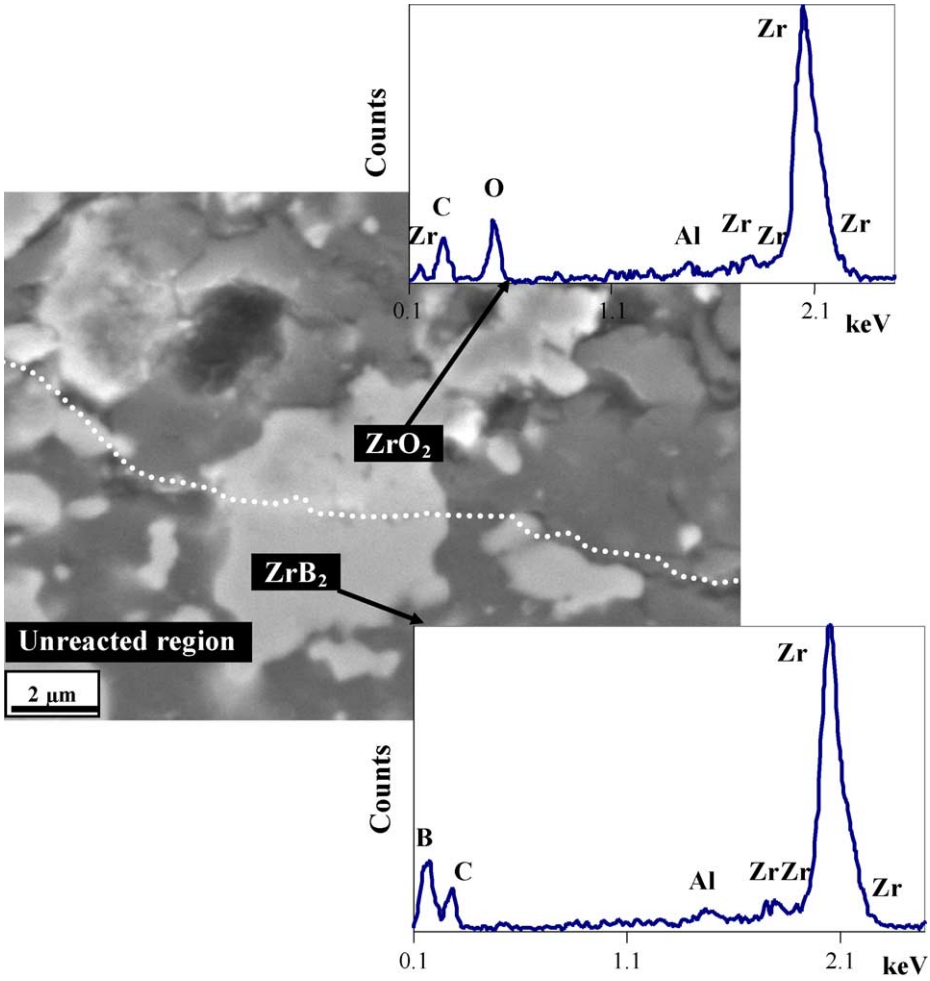

Fig. 7. SEM Micrograph of the cross-section and EDS Spectrums: limit between the oxide layer and the unreacted bulk after oxidation at 1200 °C.

with the AlN–SiC matrix of the composite. The crystals dimensions increase with increasing the oxidation temperature. According to X-ray diffraction, this phase is aluminium borate with stoichiometry $2Al_2O_3{\cdot}B_2O_3$. The peak intensity, very low in the pattern of the surface oxidized at 900 °C, increases with increasing oxidation temperature. Monoclinic zirconia crystals (preferentially oriented along the (−1 1 1) plane) pile up on the original ZrB_2 particles. Correspondigly, the analysis of the cross-sections after treatment at 900 °C evidences a cracked oxide layer, where cracks developed owing to volume expansion during formation of zirconia and extend into the AlN–SiC matrix (Fig. 5b). A discontinuous glassy phase is present and rapidly increases after oxidation at temperature above 1000 °C. In fact the glassy layer, developed during oxidation at 1100 °C (Fig. 5c), covers the outer part of the scale, partially healing the preexisting cracks. The glassy phase contains mostly Al, Si, O and traces of boron.

The surfaces oxidized at 1200–1250–1300 °C (Fig. 4e and f) present a glassy layer, which embeds elongated crystals. According to XRD patterns, these crystal are mullite ($3Al_2O_3{\cdot}2SiO_2$,) and/or aluminum borate. The stoichiometry of aluminum borate changes from $2Al_2O_3{\cdot}B_2O_3$ in samples oxidized at 1200 °C, into $Al_{18}B_4O_{33}$ after oxidation at 1250 and 1300 °C. The relative concentrations of mullite and aluminium borate can not be determined due to the superimposition of the main peaks and the very close lattice parameters. Rounded particles of ZrO_2 are dispersed among the elongated crystals, as evidenced by the back-scattered electron image in Fig. 4e. In addition, after oxidation at 1300 °C, traces of tetragonal zirconia are also present. The cross-section of the sample oxidized at 1200 °C consists of two layers (Fig. 5d): an outer one, where zirconia crystals are dispersed in aluminosilicate/borosilicate glass (see Fig. 6 and relative EDS spectrum) and an inner one, close to the reaction interface,

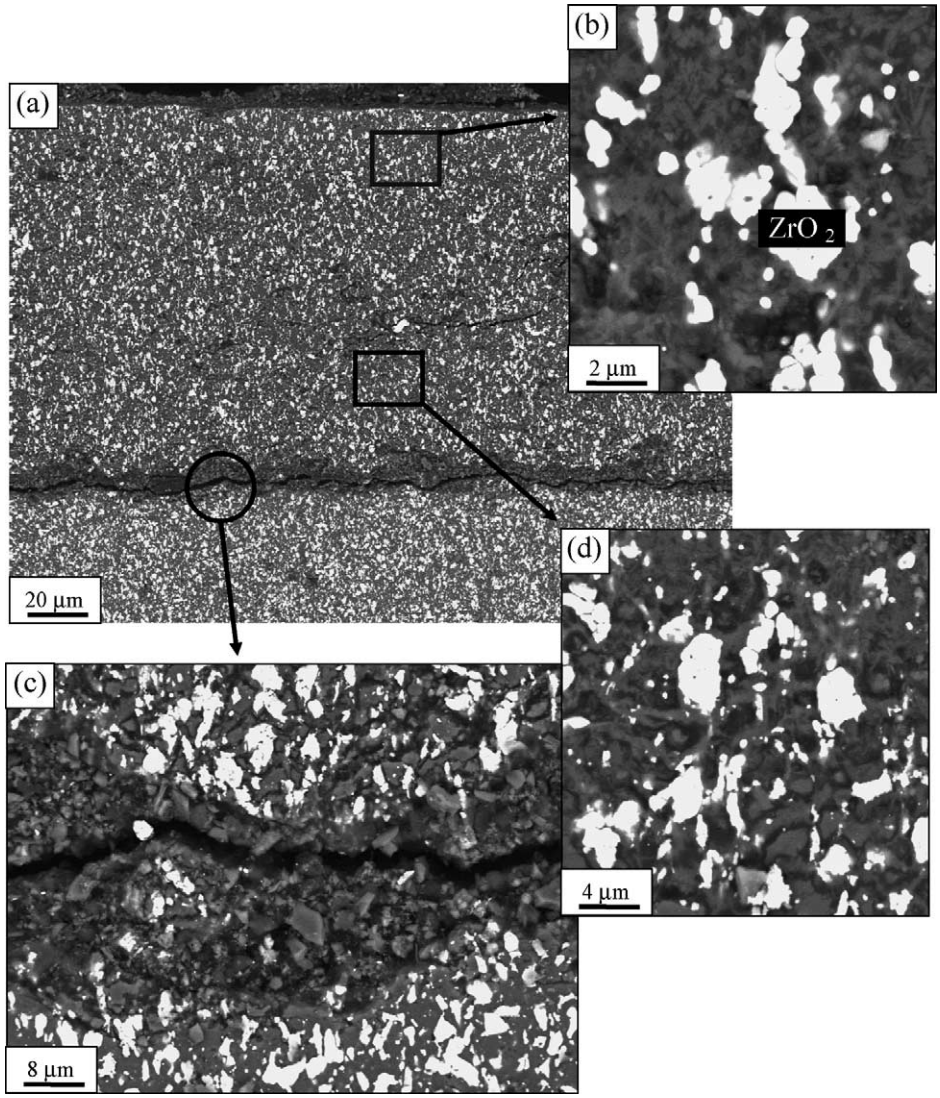

Fig. 8. (a) SEM micrographs of the cross-section after oxidation at 1300 °C; (b) compact region; (d) porous region; (c) border between the oxide layer and the unreacted region.

which is heavily cracked. An example highlighting the location of the reaction front between the inner oxide layer and the unreacted bulk is shown in Fig. 7, with the corresponding EDS spectrum. In samples treated at 1250–1300 °C, (Fig. 5e,f and Fig. 8) the above phenomena are much more accentuated. The outer part of the oxide is a dense compact layer with crystallized elongated crystals and zirconia. The inner oxide scale has deep cracks and tends to spall, due to large thermal expansion mismatch between newly formed phases and pre-existing ones, which is not accommodated by glassy phase. For this reason, severe sample damage is observed after oxidation at 1300 °C.

4. Discussion and conclusions

Since the AlN–SiC–ZrB_2 composite is constituted of three oxidizable phases, the main reactions involved in the oxidation process are the following:

$$ZrB_2 + 5/2O_2 = ZrO_2 + B_2O_3(l) \quad (2)$$

$$B_2O_3(l) = B_2O_3(g) \quad (3)$$

$$2AlN(s) + O_2(g) = Al_2O_3(s) + N_2(g) \quad (4)$$

$$SiC(s) + 3/2O_2(g) = SiO_2(s) + CO(g) \quad (5)$$

According to microstructural observations and TG results, the oxidation behaviour of the composite can be divided into three regimes:

4.1. Regime I. 700–900 °C

In this temperature range the extent of AlN and SiC oxidation is limited, while ZrB_2 oxidizes according to the reaction (2). Boric acid has a low melting point (450 °C) and high vapour pressure, which make it vaporize at relatively low temperatures. B_2O_3, liquid at these temperatures, is known to have a protective effect, while ZrO_2 is semiprotective due to its anion deficiency.[13] Thus, in this temperature range, the oxidation of the ternary composite resembles that of a ZrB_2 monolithic material, with nearly parabolic kinetic. The multiple linear regression fit, gives a negative linear term, which could be related to the release of volatile products from the reaction (3).

Good fitting solutions (not shown) could also be obtained combining either parabolic plus logarithmic term, or linear plus logarithmic term. In this case, the logarithmic term could be related to slow surface coverage, which changes the "effective" cross-section.[12] The limited extent of oxidation in this temperature range does not allow to discriminate among these different behaviours.

4.2. Regime II. 1000–1100 °C

At 1000–1100 °C, boric acid should start to vaporize more rapidly, as previously observed for the oxidation of monolithic ZrB_2.[8–10] However, X-ray diffraction indicates that at these temperatures, B_2O_3 reacts with either AlN or Alumina forming aluminum borate according to the following reactions:

$$Al_2O_3 + B_2O_3(l) = 2Al_2O_3{\cdot}B_2O_3 \quad (6)$$

$$2AlN + 2B_2O_3 + 3/2O_2(g) = Al_2O_3{\cdot}B_2O_3 + B_2O_3 + N_2(g) \quad (7)$$

This phase was also found in the oxidation of AlN/ZrB_2 and AlN/TiB_2 composites.[14–16] Actually, from thermodynamic point of view, reaction (6) is highly favoured because it requires a much lower energy compared to reaction (7).[15] We observed aluminum borate to form above 900 °C, i.e. when massive oxidation of AlN into Alumina takes place. The phase diagram Al_2O_3–B_2O_3[17] indicates that up to 1035 °C, an aluminum borate with different stoichiometry can exist, i.e. $Al_{18}B_4O_{33}$. However, in our samples oxidised up to 1200 °C, this phase was not observed. Another concurrent phenomenon at 1000–1100 °C is the oxidation of SiC into silica, which further reacts forming alumino-silicate and borosilicate glasses. The formation of crystalline aluminum borate and borosilicate glass reduces the vaporization of B_2O_3 and exerts a protecting effect, thus lowering the oxidation rate. Microstructural observations are in agreement with the interpretation of the kinetic curves at these temperatures. Thanks to the presence of protective phases, the weight gain at 1000 °C is lower than at 900 °C and the kinetic curves present an asymptotic behaviour, which largely deviates from a parabolic kinetic. The logarithmic term, found in the fitting equations, can be associated to the crystallization of aluminum borate and/or scale closure. The small negative linear term, at 1000 °C could be associated with vaporization of B_2O_3, which is, instead, completely suppressed during oxidation at 1100 °C.

4.3. Regime III. 1200–1300 °C

The aluminum borate of reaction (6) reacts further with liquid boria to form a different stoichiometry:

$$2Al_2O_3{\cdot}B_2O_3 + B_2O_3(l) = Al_{18}B_4O_{33} \quad (8)$$

as predicted by the Al_2O_3–B_2O_3 phase diagram.[17] At the same time, silica reacts with alumina to form mullite according to:

$$3Al_2O_3 + 2SiO_2 = 3Al_2O_3{\cdot}2SiO_2 \quad (9)$$

These oxidation products should be protecting, however, the formation of cracks and voids causes the exposure of fresh unprotected material surface to the oxidation environment and, consequently, enhances the sample degradation, especially at 1300 °C. This behaviour is confirmed by the kinetic curves, which contain a parabolic term, related to the diffusion of oxygen into the oxide layer, and a linear term, accounting for interface reaction.

The study evidenced that the critical phase for the oxidation resistance of the tested composite is ZrB_2. A comparison with previous results, on the oxidation of an AlN–SiC composite[18] in the same operating conditions of the present study, highlights that the lower performance of the ternary composite is particularly evident at temperatures above 1100 °C. The AlN–SiC composite does not reveal detectable oxide scales during oxidation up to 1200 °C and develops an oxide layer with thickness of 10 μm after exposition of 30 h at 1300 °C. Under the same conditions the AlN–SiC–ZrB_2 composite has a surface oxide scale of about 230 μm. Another study[16] reports the oxidation of a ternary composite AlN–SiC–ZrB_2 containing only 9 wt.% of ZrB_2: the lower amount of this phase results in a better oxidation resistance of the material, which is considered suitable for applications up to 1350 °C. The main factors determining the rapid degradation of the ternary composite are the micro-cracking that follows the reaction of ZrB_2 to ZrO_2 and the role of liquid boria, which enhances the formation of a low viscosity liquid glass particularly at temperatures above 1100 °C. The liquid glass easily penetrates into the bulk through open channels and voids deriving from the oxidation of ZrB_2, and it acts as medium for the fast transport of oxygen to internal regions, inducing a subsurface oxidation.

1100 °C can be considered a limit temperature, below which the composite is suitable for applications characterized by long-term heating in air or by cyclic heating and cooling steps.

Above 1100 °C, the time of exposure becomes a critical factor. In the case of relatively low periods at high temperature, applications can be attempted up to 1400 °C, as demonstrated by the notably high bending strength value (508 MPa) obtained with tests carried out in air at this temperature.

Acknowledgements

The work is supported by the European Project Research Training Network HPRN-CT-2000-00044 “Composite Corrosion”. The research contract of M. Brach is funded by the same Project. The Authors wish to thank D. Dalle Fabbriche for the execution of the hot pressing cycle, C. Melandri and S. Guicciardi for the measurement of mechanical properties.

References

1. Sciti, D., Melandri, C. and Bellosi, A., Properties of ZrB_2-reinforced ternary composites. *Adv. Eng. Mater.*, 2004, **6**(9), 775–781.
2. Lavrenko, V. A. and Alexeev, A. F., Oxidation of sintered aluminum nitride. *Ceram. Int.*, 1983, **9**(3), 80–82.
3. Bellosi, A., Landi, E. and Tampieri, A., Oxidation behaviour of aluminum nitride. *J. Mater. Res.*, 1993, **8**(3), 565.
4. Kim, H. E. and Moorhead, A. J., Oxidation behaviour and flexural strength of aluminum nitride exposed to air at elevated temperatures. *J. Am. Ceram. Soc.*, 1994, **77**(4), 1037–1041.
5. Costello, J. A. and Tressler, R. E., Oxidation kinetics of hot-pressed and sintered α-SiC. *J. Am. Ceram. Soc.*, 1981, **64**(6), 327–331.
6. Singhal, S. C., Oxidation kinetics of hot-pressed silicon carbide. *J. Mater. Sci.*, 1976, **11**, 1246–1253.
7. Luthra, K. L., Some new perspectives on oxidation of silicon carbide and silicon nitride. *J. Am. Ceram. Soc.*, 1991, **74**(5), 1095–1103.
8. Tripp, W. C. and Graham, H. C., Thermogravimetric study of the oxidation of ZrB_2 in the temperature range of 800 °C to 1500 °C. *J. Electrochem. Soc.*, 1971, **118**(7), 1195–1199.
9. Tripp, W. C., Davis, H. H. and Graham, H. C., Effect of an SiC addition on the oxidation of ZrB_2. *Ceram. Bull.*, 1973, **52**(8), 612–616.
10. Opeka, M. M., Talmy, I. G., Wuchina, E. J., Zaykoski, J. A. and Causey, S. J., Mechanical, thermal and oxidation properties of refractory hafnium and zirconium compounds. *J. Eur. Ceram. Soc.*, 1999, **19**, 2405–2414.
11. Monteverde, F. and Bellosi, A., Oxidation of ZrB_2-based ceramics in dry air. *J. Electrochem. Soc.*, 2003, **150**(11), 552–559.
12. Nickel, K. G., Multiple Law modeling for the oxidation of advanced ceramics and a model-independent figure of merit. In *Corrosion of Advanced Ceramics*, ed. K. G. Nickel. Kluwer Academic Publishers, Norwell, MA, 1994, p. 59.
13. Bunduschuh, K. and Schütze, M., *Mater. Corros.*, 2001, **52**, 204.
14. Lavrenko, V. A., Panasyuk, A. D. and Smirnov, V. P., High-temperature oxidation of AlN–ZrB_2 ceramics. In *Key Engineering Materials, Vols. 132–136*, ed. P. Abelard, J. Baxter and D. Bortzmeyer. Trans Tech Publications, Switzerland, 1997, pp. 1625–1628.
15. Schneider, S. V., Desmaison-Brut, M., Gogotsi, Y. G. and Desmaison, J., Oxidation behavior of a hot isostatically pressed TiB_2–AlN composite. In *Key Engineering Materials, Vol. 113*, ed. R. J. Fordham, D. J. Baxter and T. Graziani. Trans Tech Publications, Switzerland, 1996, pp. 49–58.
16. Desmaison, J. and Desmaison-Brut, M., High temperature oxidation kinetics of non-oxide monolithic ad particulate composite ceramics. *Mater. Sci. Forum*, 2001, **369–372**, 59–64.
17. Levin, E. M., Robbins, C. R., McMurdie, H. F., Phase Diagrams for Ceramists. Edited and published by The American Ceramic Society, Westerville OH, 1964 (fig. 308).
18. Sciti, D., Winterhalter, F. and Bellosi, A., Oxidation behaviour of a pressureless sintered AlN–SiC composite. *J. Mater. Sci.*, 2004, **39**, 6965–6973.